

Study of Interfacial Rheology of Human Serum Albumin Microcapsules using Electrodeformation Technique

Sneha Puri and Rochish M. Thaokar

E-mail: rochish@che.iitb.ac.in

Phone: +91 (22) 2576 7241 Fax: +91 (22) 2572 6895

Department of Chemical Engineering,
Indian Institute of Technology Bombay, Mumbai-400076

August 9, 2022

Abstract

Understanding the mechanical characterization of microcapsules is critical for their precise applications, such as in pharmaceuticals, cosmetics, agriculture, food industries, etc. Microcapsules synthesized from different materials show distinct mechanical characteristics. It is therefore necessary to study these systems considering their respective micro-physics for an exact theoretical model suitable to these systems. In the present work, we conducted mechanical characterization of the membrane of human serum albumin (HSA) microcapsules using the electrodeformation technique. Proteins are widely used as encapsulating materials for many biomedical and food industries. Relating the microstructure to the mechanical properties of a protein-membrane is a challenge owing to its complex structure and sensitivity towards different environmental conditions such as pH, temperature, and solvents. Interfacial rheology of human serum albumin microcapsules studied using the electrodeformation technique shows that HSA capsules are strain-softening in nature. The viscoelasto-electrohydrodynamic model was utilized to understand the creep mechanism in the human serum albumin capsules. The effect of different reaction parameters such as protein concentration and pH on the morphology of the capsule membrane was investigated, and an attempt has been made to correlate microstructure with the mechanical properties. The pH has a remarkable effect on the morphology of HSA microcapsules which is also reflected in their mechanical characteristics. The capsule synthesized with carbonate buffer shows very distinct morphology with pores on the membrane surface, making the membrane less elastic with significant nonrecoverable creep. The capsules synthesized with different protein concentrations at the same pH condition show different morphology and thus different rheological properties. Capsules with a low concentration of HSA show smooth membrane structure with higher Young's modulus than

the capsules synthesized at a very high concentration which show a rough folded wavy structure with low membrane elastic modulus. The effect of frequency on the interfacial rheological properties of human serum albumin capsules was studied using a frequency sweep test using the electrodeformation technique. The rheological properties were computed incorporating the viscoelasto-electrohydrodynamic model for the oscillatory response of capsules. The results show that the elastic response dominates in the high-frequency regime. Thus the electrodeformation technique allows studying the effect of very high-frequency 1 Hz to 1 kHz, which is otherwise not possible with the conventional rheometers.

1 Introduction

A microcapsule is a liquid droplet covered with a thin sheet (shell) of self-assembled or crosslinked particles or polymers of a few 10s of microns in size. Common examples of natural microcapsules include red blood cells, fat globules in milk, etc. Synthetic microcapsules made up of crosslinked polymers find tremendous use in several applications. Specifically, crosslinked proteins as the shell material have attractive applications in the biomedical, pharmaceuticals, cosmetics and food industries. This paper demonstrates an electrodeformation technique to study the interfacial rheology of human serum albumin microcapsules. HSA is a biocompatible protein and having a very attractive binding capacity to many drugs. Below we briefly discuss the studies on the characterization of human serum albumin microcapsules.

The fourier transform infrared (FTIR) spectroscopic studies on HSA capsules synthesized by the emulsification method showed the participation of amino, hydroxyl, and carboxyl functional groups of albumin in the formation of the crosslinked HSA microcapsules [29]. The extent of involvement of these functional groups depends on the reaction conditions during the capsule synthesis process. Levy et al. [29] studied the chemical characterization of HSA capsules using FTIR spectroscopy and TNBS titration techniques. Their method was focused on the determination of the amount of free amino groups of the microcapsules, using the TNBS titration method to understand the degree of crosslinking, and the FTIR technique for the involvement of various functional groups at different reaction conditions.

Proteins are known to be sensitive to pH and acquire a configuration that depends upon the protonation/deprotonation of amino groups and ionization of their carboxylic group present on the amino acid side groups [16]. At low pH, the involvement of only free amine groups is seen, whereas, for high pH, carboxyl and hydroxyl groups also participate in the reaction. Moreover, at a higher pH, the ionization of the amine groups is suppressed, thereby favoring the amide reaction with the reducing agent. HSA capsules synthesized with phosphate buffer in the pH range between 5.9 to 8 yielded larger-sized microcapsule aggregates with smooth morphology that collapsed after drying. However, with a similar reaction condition, microcapsules prepared with a carbonate buffer (pH 9 to 11) resulted in smaller, pale yellow, rough individual spherical capsules [29].

In yet another study, it was found that the acylation of amino groups of HSA is more intense with acetate buffer than with the phosphate buffer at the same pH of 5.9 [18]. This gives the advantage of increasing crosslinking density of the membrane of HSA microcapsules without raising the pH. The difference between acetate and carbonate buffers was attributed to the difference in the ionic concentration of the two buffers. The exact reason for why the higher ionic concentration of the acetate buffer favors acylation of the amino groups at the same pH though is unclear.

Increasing reaction time shows a similar effect as upon increase in pH on membrane morphology of the capsules. At pH 9.8 (carbonate buffer) with 2 min reaction time, bigger $\sim 30 \mu m$ capsules with smooth membrane morphology is formed, while as the reaction time increases, smaller microcapsules with rough morphology are obtained. Initially, only free amines participate in the reaction, and as the reaction time increases, more functional groups are involved in the reaction producing rough and more granular microcapsules [30]. Similarly, with the increase in the concentration of crosslinker, a rough membrane is formed, showing a higher degree of crosslinking [30, 29].

To summarize, the literature survey about the synthesis of HSA capsules indicates that two types of capsules can be synthesized by tuning the different reaction parameters.

1. Poorly crosslinked type-1 capsules that show smooth membrane morphology and involve mainly the reaction of free amines; can be synthesized either at low pH, at low TC concentration (2.5 percent), or with a short reaction time at high pH. The extent of crosslinking is much lower in this case.
2. Highly crosslinked type-2 capsules are smaller in size with rough morphology and involve the formation of more β sheets, ester, and anhydride bonds and can be synthesized by intensifying the reaction by increasing one of the reaction parameters; pH, reaction time, or TC concentration.

Designing a microcapsule with desired mechanical characteristics is a challenge in microencapsulation technology. The capsules prepared with different materials, such as chitosan, alginate, and proteins, show distinct membrane mechanical properties. For example, HSA-alginate capsules show strain hardening [5] behavior while serum albumin (HSA/BSA) capsules exhibit strain-softening nature [20, 21]. The reaction parameters and fabrication techniques can also significantly affect the membrane properties of microcapsules synthesized with the same system. Therefore it is often necessary to study their properties on a case-by-case basis to understand their characteristics that are relevant to their applications.

Mechanical characterization of water-in-water albumin capsules using the microfluidic technique has been reported in several studies [12, 13, 19, 21]. Various theoretical models such as Hooke's law, Neo-Hookean, and Skalak law describe the 2D membrane characteristics of elastic microcapsules. Most of the literature studies considered strain-softening Neo-Hookean law to compute mechanical properties of albumin capsules [21, 20], barring the study about

stretching of HSA capsules in planar elongation flow by De Loubens et al. [13] which reports that these capsules follow generalized Hooke’s law with Poisson’s ratio of 0.4 [13].

The deformation study of HSA capsules in elongational flow and the atomic force microscopy (AFM) technique allowed the estimation of surface shear modulus and 3-D Young’s modulus in the small deformation limit. A combination of these two methods revealed that Young’s modulus and membrane thickness both increase with the HSA concentration and size of the capsule [12]. Studies on the influence of protein concentration and the size of the microcapsule on the mechanical properties of the HSA microcapsule membrane using the microfluidic technique suggest that as the size and the HSA concentration increase, the shear modulus also increases [20, 21, 14]. Simultaneous fabrication and characterization of HSA microcapsules using a microfluidic (double flow-focusing setup) technique have been reported in the literature; however, it is difficult to remove the excess unreacted precursor and to make stable capsules with this technique. The study also showed that as the reticulation time increases, the shear modulus also increases [10].

Studies have been conducted on ovalbumin capsules to understand their mechanical characteristics. The study of the deformation of ovalbumin capsules under shear flow through a cylindrical microchannel at different flow rates showed that the use of a Neo Hookean law gave a constant value of shear modulus in the low deformation regime [28]. The study comparing the mechanical and chemical characterization of ovalbumin capsules, done using the microfluidic technique and combined with determining free amino groups using the TNBS method, shows that the shear modulus and the amino groups are nearly constant with the reaction pH for the capsules fabricated after 5 min of reticulation. The shear modulus increases with the reaction time, while the NH_2 content decreases with it, indicating the conversion of progressive amines to amides. An overall increase in shear modulus with pH is also observed for ovalbumin capsules, similar to the HSA capsules [9], but with an unexpected rise in NH_2 content.

Very few studies have been conducted on the viscoelastic characterization of microcapsules. The theoretical studies considered the Kelvin-Voigt model to describe the viscoelastic properties of the membrane under shear flow [2, 42]. An experimental study was performed by Chien et al. [7] on the erythrocyte membrane in which the Kelvin-Voigt model was used to find the membrane viscosity using the micropipette technique. Recently, alginate-coated chitosan capsules were studied using the microelectromechanical (MEMS) microgripper technique, and the Kelvin model was used to find the viscoelastic characteristics of these microcapsules [27]. The viscoelastic properties of oil-in-water vitamin A capsules coated with starch were studied using the four-element Burger model [43]. Similarly, urea-formaldehyde microcapsules showed viscoelastic characteristics, and the relaxation was described by the three-element Maxwell model [22]. Recently, a novel method has been developed, by integrating a deep convolutional neural network with a high-fidelity mechanistic capsule model, to predict the membrane viscosity and elasticity of a microcapsule from its dynamic deformation when flowing in a branched microchannel [32].

Only a few studies have been reported on the viscoelastic properties of water-in-water HSA microcapsules. The study of tank treading motion of HSA microcapsules indicates that these capsule membranes are viscoelastic in nature, and the membrane viscosity was computed from the measurement of the period of rotation of the membrane [14]. The transient response of cross-linked HSA capsules was studied by flowing capsules through a sudden expansion, and comparing the characteristic time scales of the capsule relaxation with a complete numerical model of the relaxation of a capsule flowing in a rectangular channel. The study shows that the crosslinked HSA membrane is viscoelastic and that the relaxation is solely a function of the ratio of the relaxation time to the flow convective time [19].

In the present work, we use the electrodeformation technique to study the viscoelastic properties of HSA microcapsules using creep and oscillatory tests. An elasto-electrohydrodynamic model is used to compute the membrane elasticity and viscosity by correlating the fitted parameters of five element spring dashpot model. The dynamics of the deformation of the capsule was studied at constant electric stress for different frequencies to study the effect of frequency on membrane rheological properties. The electrodeformation method allows interfacial rheological studies at very high frequencies, not easily accessible in conventional interfacial rheometers.

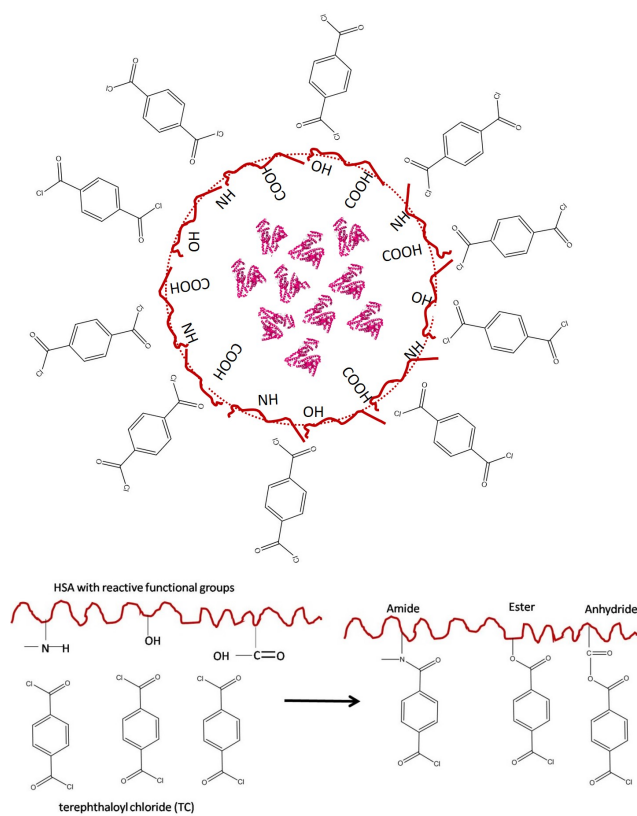
2 Materials and methods

Human serum albumin protein standard (P8119), span 85, chloroform, terephthaloylchloride, and silicone oil (350 cSt) were obtained from Sigma Aldrich. Cyclohexane was obtained from Imparta chemicals, and pH 7.4 PBS buffer from LOBA chemicals. All the chemicals were used as procured.

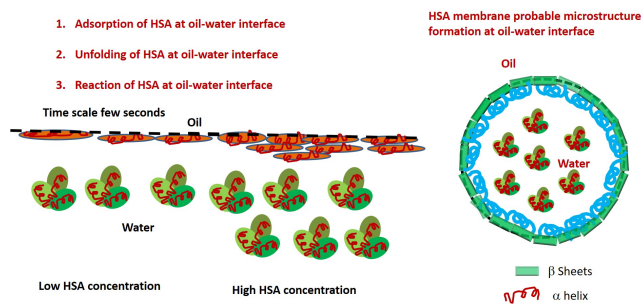
2.1 Methodology for synthesis of HSA capsules

Figure 1 shows the probable reaction mechanism for the formation of the membrane of HSA microcapsules. HSA from the aqueous phase adsorbs at the oil-water interface and subsequently unfolding of proteins can occur, making the buried functional groups, amine, ester, and hydroxylic of proteins present in the aqueous phase available for reaction with the chloride group of the crosslinker terephthaloyldichloride present in the oil phase, to form amide, ester, and anhydride bonds. Adsorption and unfolding phenomenon of a protein depend on the reaction parameters, such as protein concentration and pH. At a high concentration of HSA, there might be competition between adsorption and the unfolding process resulting in the multilayer film formation. The hydrophobic β -sheets would mostly be on the oil side and the α -helix would be on the aqueous side of the membrane.

The HSA microcapsules were synthesized by the conventional method of interfacial polymerization of HSA using the emulsification technique with terephthaloyl chloride as the crosslinking agent [29] as shown in Figure 2. The lyophilized HSA



(a)



(b)

Figure 1: Schematic representation of (a) reaction mechanism (b) membrane formation mechanism for HSA microcapsule (not to the scale)

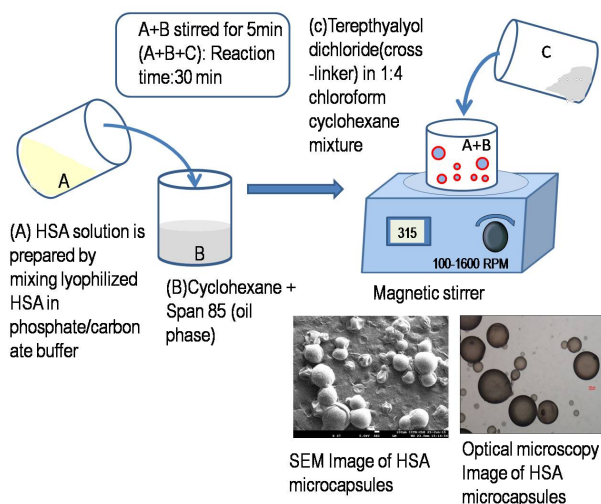


Figure 2: Methodology for the synthesis of human serum albumin microcapsules

was dissolved in the phosphate (pH 7.4) or carbonate (pH 9.2) buffer to make solutions of different [10, 20, and 30 percent (weight/volume)] concentrations of HSA. Note, % w/v = 100 gms of solute/100 ml of solution. Thus, a 10% HSA solution had 0.1 gms of HSA/100 ml of solution, or 100 mg/ml of HSA. Around 100 μ l of the HSA solution was then added to cyclohexane containing 5 percent (volume percent) span 85 and stirred at a constant speed of about 600 rpm for 5 min, to produce an emulsion of aqueous droplets containing HSA dispersed in cyclohexane. The cross-linker terephthaloyldichloride (0.25 percent weight/volume), dissolved in (1:4) chloroform cyclohexane mixture, was then added to this emulsion, and the polymerization reaction was stopped after 15 min by dilution of the reaction media. The capsules were washed gently thrice with an organic phase to remove the excess crosslinker.

In the present work, we use the notations HSA_{10} , HSA_{20} , and HSA_{30} to represent capsules synthesized with PBS buffer at pH 7.4 with concentrations of 10, 20, and 30 percent HSA respectively. A HSA capsule synthesized with carbonate buffer at pH 9.2 for 20 percent HSA is represented as $HSA_{20}, pH9.2$. Poly-dispersed microcapsules were formed by this method in the size range of 10 μ m to 400 μ m. Any one of these capsules from the emulsion was then used for more detailed interfacial study and the size of such a capsule was estimated from images obtained using light microscopy. The size distribution of the suspension of capsules (See Figure S1 provided in Supplementary Information) was studied using instrument particle size analyzer (Horiba LA 960). It should be noted here that for size measurement using the particle size analyzer, the capsules were resuspended in water, by removing the organic solvent using excess water. Thus the size of the capsules obtained using the Horiba (LA 960) are only indicative of the actual water-in-oil, crosslinked capsules, synthesized using the water-in-oil

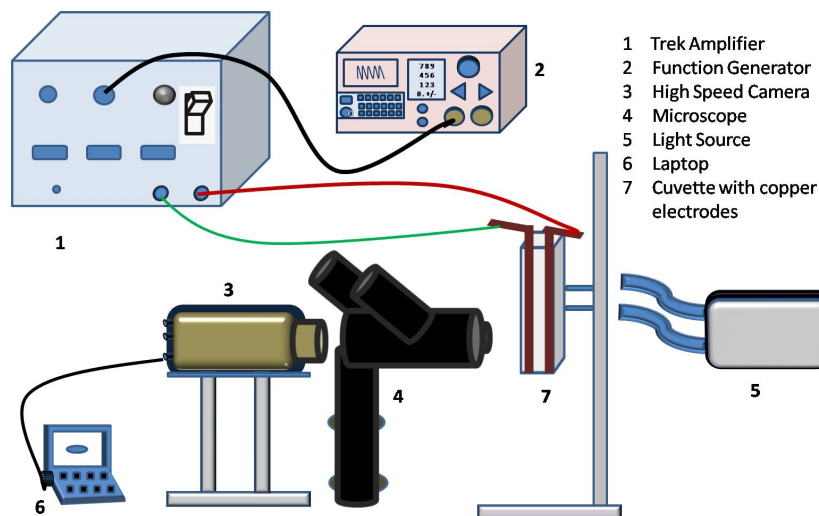


Figure 3: Electrodeformation experimental set-up

emulsion (For details see Supplementary Information).

2.2 Scanning electron microscopy (SEM) studies for HSA capsules

The morphology of microcapsules was studied using the scanning electron microscopy (SEM) technique. Freshly synthesized capsules were placed on an aluminum foil using the drop-casting method and the organic phase was evaporated at room temperature to get the dry sample. The samples were coated with platinum for 60 s. Imaging was carried out in the dry mode at 5 kV with various magnifications ranging from 45X to 50,000X.

2.3 FTIR studies on capsules

The secondary structure of proteins has been widely studied using the FTIR spectroscopic technique, especially the Amide-I, Amide-II band [37, 38, 40, 38]. The microcapsules synthesized using the method described, were centrifuged and washed thrice with the organic phase and thrice with deionized water, and finally suspended in deionized water. The lyophilized microcapsules were then studied using the standard procedure for a wavelength range of 6250 to 5882 nm using the FTIR (Bruker, Germany, 3000 Hyperion Microscope with Vertex 80 FTIR System) instrument.

2.4 Experimental set-up for electrodeformation study:

The experimental set-up (see Figure 3) consisted of two copper electrodes of 45 mm in height, 1 mm in thickness, and 1 cm wide, attached to the inner sidewalls of a plastic cuvette. The distance between the copper electrodes was kept as 4 mm. A required voltage difference was applied across the copper electrodes with the help of a function generator (33220A Agilent Technologies Pvt. Ltd., USA) that had a voltage range of 0 – 20 V. The frequency of the ac voltage used in this work, was in the range of (1Hz-1kHz). The function generator was connected to a high voltage amplifier TREK (model 20/20C-HS) of fixed gain 2000 V/V to generate the desired amplified voltage.

For the mechanical characterization, a single microcapsule was manually placed in the cuvette containing 350 cSt silicone oil with the help of a micropipette. As the electric field was applied, the capsule deformed into an ellipsoidal shape in the direction of the field. The complete electrodeformation video (when the field is switched on and also after switching off the field) was recorded with the help of a high-speed videography (by Phantom V12 camera), attached to a stereo-microscope (Leica z16AP0) at 200 – 70000 frames per second. A light source (Nikon) was used for illumination and image analysis was performed using the ImageJ software (<https://imagej.nih.gov/ij/>).

The deformation of the microcapsules was estimated by defining a modified Taylor parameter.

$$D = \frac{((l/L) - (b/B))}{((l/L) + (b/B))} \quad (1)$$

Where L, B, l, and b are the initial major and minor axes of the original undeformed and deformed capsule before and after the application of the electric field respectively. The surface Young's modulus is calculated using Eq.2 (See [26] for details), which relates electric capillary number (Ca_e) to deformation (D), as expressed below.

$$D = \frac{16}{45} Ca_e \quad (2)$$

$$Ca_e = \frac{a E_o^2 \epsilon \epsilon_o}{E_s} \quad (3)$$

Here, E_o is the RMS value of the applied electric field, a is the radius of a capsule, ϵ_o is permittivity of free space, ϵ is the dielectric constant of the medium and E_s is the surface Young's modulus of a membrane (N/m).

2.5 Viscoelastic model for the study of rheological properties of microcapsules

In the present work, we describe the rheological characteristics of the human serum albumin capsules using the five-element Burger model. The five-element viscoelastic model (Figure 4) consists of two Kelvin-Voigt elements and one dash-pot arranged in series used for fitting the deformation versus time data for

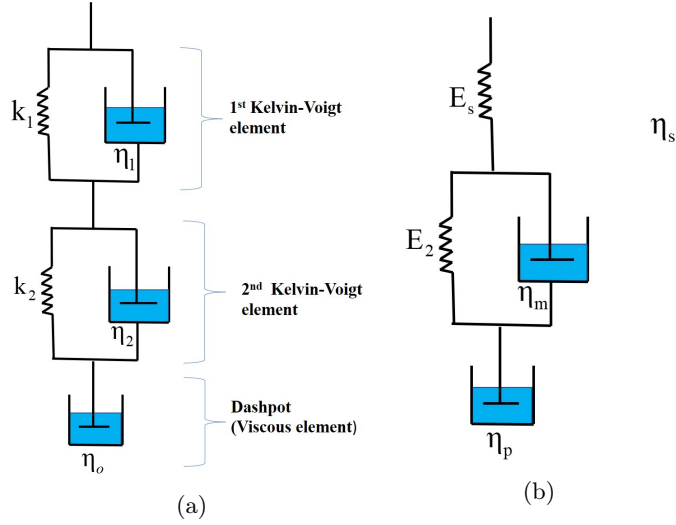


Figure 4: (a) Schematic of spring-dashpot visco-elastic model (b) Corresponding schematic of stress-strain constitutive equation for elasto-electro-hydrodynamic model

creep experiments. The complete response, that is deformation with respect to time, for a step-stress is proportional to $a\epsilon\epsilon_e E_o^2$ for $t < t_o$ is given by,

$$D(t) = \left(\frac{1}{k_1} \left(1 - e^{-t/\tau_1} \right) + \frac{1}{k_2} \left(1 - e^{-t/\tau_2} \right) + \frac{t}{\eta_o} \right) a\epsilon\epsilon_e E_o^2 \quad (4)$$

and for $t > t_o$

$$D(t) = \left(\frac{1}{k_1} \left(e^{-(t-t_o)/\tau_1} - e^{-t/\tau_1} \right) + \frac{1}{k_2} \left(e^{-(t-t_o)/\tau_2} - e^{-t/\tau_2} \right) + \frac{t_o}{\eta_o} \right) a\epsilon\epsilon_e E_o^2 \quad (5)$$

where $\tau_1 = \eta_1/k_1$ and $\tau_2 = k_2/\eta_2$.

Note that the elastic and viscous constants k_1 , k_2 , η_1 , η_2 , in the spring-dashpot model, do not exactly represent membrane elasticity and viscosity. It is expected that η_1 , η_2 should represent the solution viscosity $a\mu_e$ shown in Figure 4 (b)) and membrane viscosity η_m , respectively, with k_1 , k_2 , representing the membrane surface elasticity. A more accurate way is to have these spring-dashpot constants expressed as equivalent frame invariant stress-strain measures, which when solved in the spherical coordinate system, yield non-trivial geometry and property dependent parameters (such as viscosity ratio etc).

Therefore an viscoelasto-electrohydrodynamic model developed in our earlier work [35] which relates the parameters of the spring dash-pot model with the elasticity, membrane viscosity and solution viscosity as mentioned earlier, that

is $\eta_1 \sim \mu_e a$ and $\eta_2 \sim \eta_m$, while $k_1 \sim E_s$ and $k_2 \sim E_y$ is used. The interfacial stress-strain relationship for this 4-element linearised elastic model is given by,

$$\tau_{\theta\theta}^{el} + 2 \frac{E_s \eta_p + E_s \eta_m + E_2 \eta_p}{E_s E_2} \frac{\tau_{\theta\theta}^{el}}{dt} + \frac{\eta_m \eta_p}{E_s E_2} \frac{d^2 \tau_{\theta\theta}^{el}}{dt^2} = \eta_p \frac{d\epsilon_{\theta\theta}}{dt} + \frac{\eta_m \eta_p}{E_2} \frac{d^2 \epsilon_{\theta\theta}}{dt^2} \quad (6)$$

$$\tau_{\phi\phi}^{el} + 2 \frac{E_s \eta_p + E_s \eta_m + E_2 \eta_p}{E_s E_2} \frac{\tau_{\phi\phi}^{el}}{dt} + \frac{\eta_m \eta_p}{E_s E_2} \frac{d^2 \tau_{\phi\phi}^{el}}{dt^2} = \eta_p \frac{d\epsilon_{\phi\phi}}{dt} + \frac{\eta_m \eta_p}{E_2} \frac{d^2 \epsilon_{\phi\phi}}{dt^2} \quad (7)$$

where subscripts " $\phi\phi$ " and " $\theta\theta$ " represent the azimuthal and meridional quantities, and $\epsilon_{\theta,\theta}$, $\epsilon_{\phi,\phi}$ represent the linearised strain. This coupled with the electric and hydrodynamic stresses yields a relationship between the capsule deformation and the elastic, electric, and hydrodynamic parameters. The detailed model derivation is described in the Supplementary Information of our previous work [35].

The equations (4, 5) were fitted (Figure 12) using the MATLAB2019a and the parameters k_1, k_2, η_1, η_2 , and η_o were estimated. The estimated fitting parameters are related to the elasticity, membrane viscosity, solution viscosity by the detailed viscoelasto-electrohydrodynamic model as mentioned in the Eq. 8.

$$k_1 = \frac{16E_s}{45}; \quad k_2 = \frac{16E_y}{45}; \quad \eta_1 = \frac{64a\mu_e}{105} \quad \eta_2 = \frac{32\eta_m}{45}; \quad \eta_o = \frac{32\eta_p}{45}; \quad (8)$$

2.6 Viscoelasto-electrohydrodynamic model for oscillatory test

The effect of frequency on the viscoelastic properties such as elasticity and membrane viscosity was studied by applying an oscillatory (ac) electric field, of varying frequencies, to the HSA microcapsules. The equations can be solved using the Laplace Transform technique when a sinusoidal electric field is applied. The equivalence between the complete hydrodynamic model and the spring-dashpot Burgers model is again found to exist similar to that of step stress case and the response is given by

$$\begin{aligned} (D/a\epsilon\epsilon_o E_o^2) = & \frac{1}{2k_1} + \frac{1}{2k_2} + \frac{t}{2\eta_3} - \frac{2\tau_1^2 \omega^2 e^{-\frac{t}{\tau_1}}}{4k_1 \tau_1^2 \omega^2 + k_1} - \frac{2\tau_2^2 \omega^2 e^{-\frac{t}{\tau_2}}}{4k_2 \tau_2^2 \omega^2 + k_2} \\ & \left(\frac{1}{2(4k_1 \tau_1^2 \omega^2 + k_1)} + \frac{1}{2(4k_2 \tau_2^2 \omega^2 + k_2)} \right) \cos(2\omega t) + \\ & \left(-\frac{1}{4\eta_3 \omega} - \frac{\tau_1 \omega}{4k_1 \tau_1^2 \omega^2 + k_1} - \frac{\tau_2 \omega}{4k_2 \tau_2^2 \omega^2 + k_2} \right) \sin(2\omega t) \end{aligned} \quad (9)$$

where the relationship between the parameters of the spring dashpot Burgers model to that of the full viscoelasto-electrohydrodynamic model remains the same.

The above expression can be used to fit and estimate the E_s, E_y, η_m and η_p values from the deformation time series for each frequency.

2.7 Methodology for estimation of model parameters and confidence bounds

The variation of $J(t)$ (ratio of deformation to electric stress) with time was fitted using the equations 4, 5 and 8 to estimate the model parameters using MATLAB R2019a and `Fminsearchbnd` [17] method for each capsule. The rheological properties of HSA capsules was estimated by fitting the mean deformation of all capsules for estimating the rheological properties from the fitting of plotted mean deformation with respect to stress. The confidence bounds were estimated for the parameters estimated from mean deformation of all capsules. We computed the confidence bounds for the estimated parameters using the F test [34].

3 Results and discussion:

3.1 Different time scales in the system

The formation of a cross-linked protein film at an oil-water interface proceeds through several steps at different rates. When proteins are dispersed in an aqueous solution, they can self-aggregate. The time scale of self-aggregation of HSA molecules to form oligomers seems to be of the order of few microseconds, indicating that the formation is instantaneous, and aggregate sizes of around a few hundred nanometers have been reported[11]. The aggregated and non-aggregated protein molecules then migrate to the oil-water interface over time scales of $a^2/D \sim (300\mu m)^2/(6 \times 10^{-11}) \sim 1500s$. The time scale though could be shorter because of convection in the system on account of stirring as well as very high concentrations of HSA used in this work, which can effectively decrease intermolecular and interaggregate distance as well as their distance from the interface.

The second relevant time scale is that of adsorption of proteins on the surface. This is reported to be of the order of 1 s [41]. This is followed by protein unfolding, at the oil-water interface, which is known to occur over time scales of few seconds to minutes. Finally the crosslinking is expected to be instantaneous due to very fast reaction. Further, growth of the interfacial film can occur due to diffusion-controlled reaction since the HSA present inside the drop phase needs to overcome the barrier of the polymeric membrane formed to react further with the cross-linker present on the oil side. The other time scale of relevance, which is the diffusion time of TC to arrive at the interface is expected to be very short.

3.2 Characterization of capsules using Fourier transform infrared spectroscopy (FTIR) technique:

The amide -I band ($1600-1700\text{ cm}^{-1}$), which has contributions from the $C=O$ stretching due to vibration of the amide group, the in-phase bending of the N-H bond and the stretching of the C-N bond, is the most sensitive spectral region representing changes in secondary structure of proteins [40]. Amide-II is derived mainly from in-plane N-H bending and the C-N stretching vibrations and is more

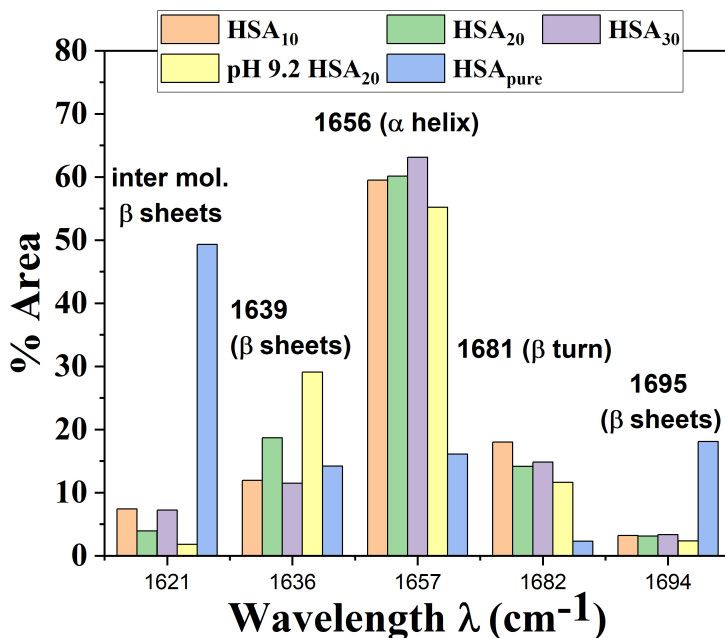


Figure 5: Comparison of secondary structure of original HSA and HSA capsules synthesized at different conditions

complex than Amide-I. Although this band is conformationally sensitive, it has not been commonly used for describing changes in protein structures. The other amide bands are rarely used to study protein structure due to their complexity and dependence on the details of the force field, the nature of side chains, and hydrogen bonding[40].

Figure S2 provided in Supplementary Information shows FTIR spectra in full-range for pure HSA and cross-linked HSA microcapsules studied in the present work. We analyzed the Amide-I band in detail to understand the microstructure of the membrane of the microcapsules using quantitative analysis of the Amide-I band contour, employing curve fitting, second derivative, and Fourier self-deconvolution methods. A Gaussian curve-fitting was conducted on deconvoluted spectra using OriginPro 2019b software. The peaks obtained by deconvolution of the amide-I band are assigned to specific types of secondary structure based on the known correlations between different secondary structures (α helix, β sheets, random coil) of proteins and their FTIR spectra [29, 33, 37].

From Figure S2 (See Supplementary Information), it is clear that there is a significant difference in the spectral peaks for uncrosslinked HSA in aqueous solution and cross-linked capsules. The deconvoluted Amide-I bandwidth spectra fitted for different cases of capsules as well as that of lyophilized uncrosslinked

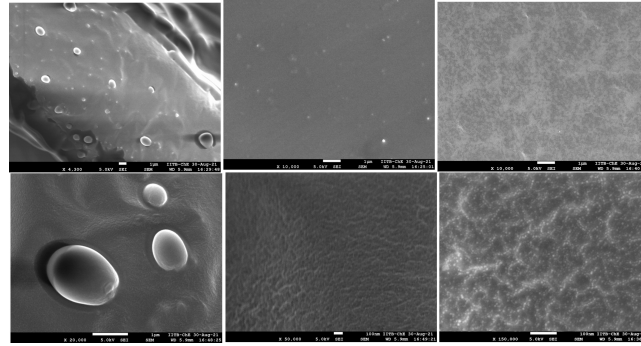
HSA is shown in Figure S3 and S4 provided in Supplementary Information. Figure 5 shows percentages of different elemental structures such as α -helix, β -sheets and random coils present in the capsules for different cases considered in the present study. It is important to note here that although the aqueous HSA molecules contain no β -sheets and have a completely helical structure, the lyophilized HSA used in our FTIR study showed a significant percentage of β -sheets. Infact, Figure 5 indicates that the pure lyophilized HSA contains more β -sheets than the crosslinked HSA capsules. It is known that lyophilization of protein leads to unfolding and changes in their secondary structure, which upon rehydration in an aqueous buffer, might be again refolded entirely or partially [31].

The capsules synthesized with pH 9.4 buffer showed more β -sheet formation than the capsules synthesized with PBS 7.4 buffer. This could be attributed to greater disruption of the native structure at higher pH due to charge repulsion. It should be noted that the FTIR study was done on lyophilized capsules with polydispersed capsules synthesized by the emulsion technique. Therefore the variation of β sheets with concentration at pH 7.4 can not be accounted due to polydispersity in the size of capsules. The results of FTIR studies for different concentrations of HSA should be analyzed with caution. The FTIR studies were conducted on a collection of capsules of varying sizes, as obtained in the emulsion technique. As shown later in the studies, the radius of the capsule can affect the crosslinking significantly. The different percentages of α -helix, β -sheets, and random coil in capsules can result in different membrane surface morphologies, which ultimately affect their mechanical properties. At low pH, free amines participate in the reaction while at higher pH, the carboxylic groups can ionise and participate in anhydride bond formation along with ester bonds formed by acylation of hydroxyl groups [29]. The involvement of different functional groups in the crosslinking could affect the crosslinking degree and formation of secondary protein structure.

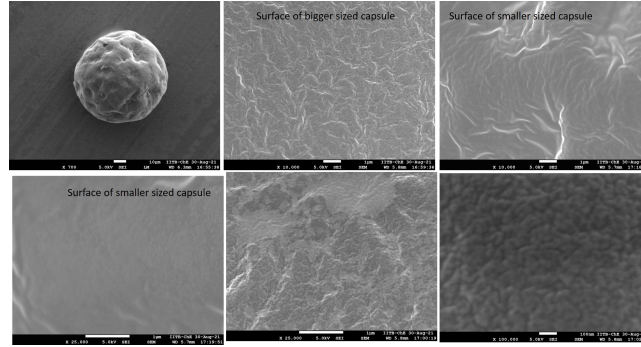
3.3 Scanning electron microscopic results for membrane surface morphology

Figure 6 shows the surface morphology of the microcapsule membrane for different pH and concentrations of HSA studied in the present work using SEM images. The different morphologies of capsules for different HSA concentrations could be due to the fact that the interfacial adsorption and unfolding phenomena depend upon the pH and concentration of HSA. These factors affect the cross-linking and thereby, the membrane morphology. The degree of cross-linking reaction and membrane microstructure depends upon the availability of buried functional groups of a protein at the interface. This in turn depends upon the protein conformational changes induced by a change in interface environments such as pH, HSA molecules per unit area, and the nature of the interface (aqueous, organic, air).

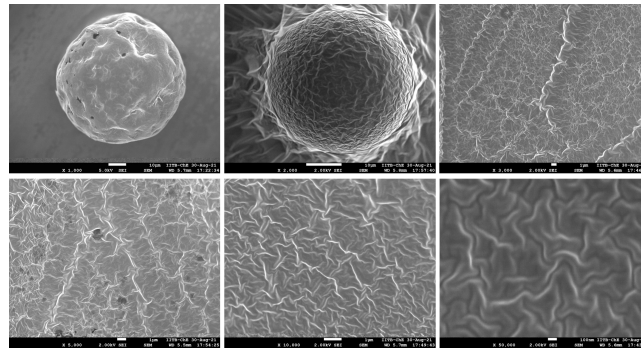
Figure 6 indicates that HSA_{10} capsules show relatively smoother morphology than that for the other cases. SEM images showed that tiny microcapsules are



(a)



(b)



(c)

Figure 6: Scanning electron microscopy images for capsules prepared with 15 min reaction time with phosphate pH 7.4 buffer for (a) HSA_{10} (b) HSA_{20} (c) HSA_{30}

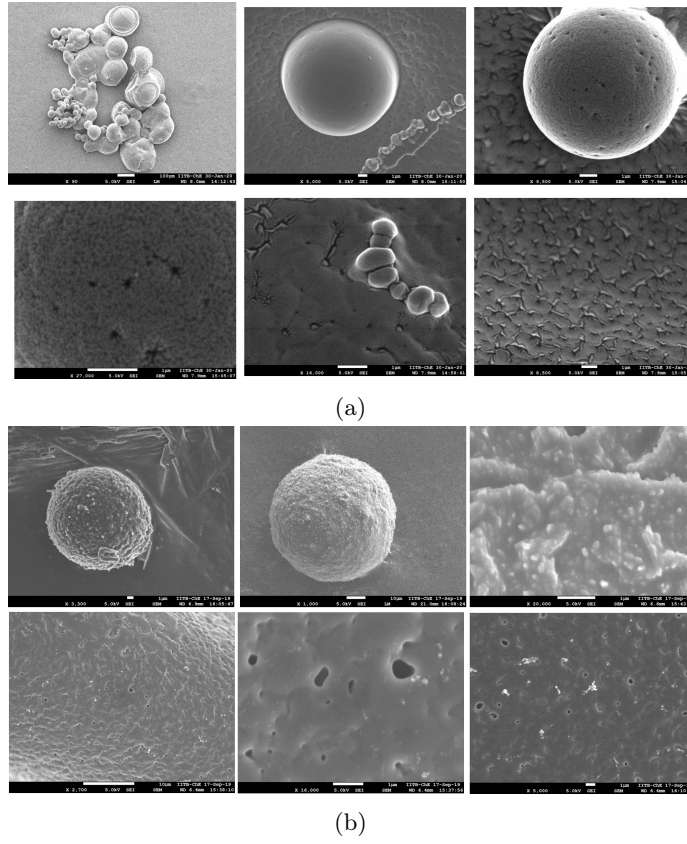


Figure 7: Scanning electron microscopy images of HSA capsules synthesized with carbonate buffer at pH 9.2 (a) 10 percent HSA, 20 min reaction (b) 15 percent HSA, 20 min reaction

adsorbed on the surface of bigger microcapsules in the case of HSA_{10} . The adsorbed smaller capsules show very smooth membrane surface morphology. This is possibly because the surface concentration of the protein $\Gamma = 4/3 a C$, where C is the bulk HSA concentration for a capsule with size a . Thus reduction in size leads to lower surface concentration, lower reaction rates, and thereby lower crosslinking and a smoother surface, aided by lower surface concentration. It should be mentioned here that the capsules synthesized with the emulsification method give a wide range of size distribution, and hence the smaller and larger microcapsules prepared with the same HSA concentration showed different morphology. Similar to HSA_{10} , smaller microcapsules with HSA_{20} also showed relatively smoother membrane morphology than bigger microcapsules.

In the case of HSA_{20} (Figure 6 b), for the similar sized capsules, the capsules showed a rougher membrane surface than for the case of HSA_{10} , possibly due to higher concentration of HSA. The microcapsules synthesized with 30% HSA concentration showed a much different microstructure (Figure 6 c) than for the other two cases (HSA_{10} and HSA_{20}). For the case of HSA_{30} , the capsules showed a wavy folded structure. Few microcapsules of HSA_{30} case showed pores on their membrane surfaces. The change in the morphology for HSA_{30} could be attributed to the formation of larger oligomeric structures in the bulk at such high concentrations. These oligomeric structures can assemble at the interface and form porous, weakly crosslinked structures.

Capsules synthesized with carbonate buffer at pH 9.2 showed a very rough, granular membrane surface with bigger pores (Figure 7), identical to those seen for HSA_{30} . It is known that HSA changes its configuration from native form to a basic structure when pH changes from 7 to 9. This N-B transition; results in exposure of the buried residues, leading to an increase in exchangeable hydrogen and an increased bulk aggregation despite increased charge stability. This is supported by the greater conversion of α -helix to β -sheets for pH 9.4 as seen in the FTIR studies. The assembly of these bulk oligomers at the interface can lead to a porous membrane morphology. Thus both high pH and high concentration can lead to increased hydrophobicity and formation of oligomers in the bulk aqueous solution. Further, we investigate the rheological properties of HSA capsules using the electrodeformation technique.

3.4 Justification for the five-element Burger model:

The dynamic deformation of HSA capsules studied at different applied stresses shows an instantaneous deformation followed by slow time-dependent deformation. The instantaneous deformation can be related to the spring element k_1 , associated with the solution viscosity giving a fast timescale. The k_2 and membrane viscosity (η_2), correspond to a slow creep response. The nonrecoverable creep deformation, is captured by the extra dashpot in series (η_o). From a microstructural viewpoint, the occurrence of the elasticity can be attributed to the existence of intermolecular bondings. It has been suggested in the literature that the protein molecule exists on the surface in an unfolded structure, probably in the form of straightened β -configuration resulting in the instantaneous elastic response [24]. The extent

of various secondary structural units such as α -helix, β - sheets, and random coils and their conformational arrangements in cross-linked protein can result in the different rheological properties of the membrane.

The literature does not present enough evidence on structure-rheology relationships for crosslinked proteins. For example, it is unclear from the literature if the proteins at the interface are folded or unfolded and the extent of conversion of α helices into β sheets, as well as the percentage of intermolecular and intramolecular crosslinking. Based on the limited literature [44, 3, 6, 15, 8, 23, 4, 1] about the relation between different structural units of protein with the mechanical characteristics, for an interfacially crosslinked protein network, we propose a microstructure for the microcapsules as follows:

1. The interface is laden with proteins adsorbed from the bulk, either as single molecules or as oligomers.
2. The protein molecules then can unfold to varying degrees, typically, the domains I, II, and III could break the quaternary structures without significantly affecting their individual tertiary and secondary structures.
3. Increased conversion of the α -helix to the β -sheets indicates increased hydrophobicity. This could lead to a higher oligomerization in the bulk, or indicate a higher amount of unfolding at the interface, with hydrophobic parts residing in the oil phase.
4. The unfolded structures could get crosslinked, most likely in the bulk, with the hydrophobic regions of the proteins anchored in the oil phase.
5. The interfacial film is typically multi-layered. The microstructure of the interfacial film and its crosslinking determines the rheological properties of the microcapsule. Multilayered and thick films are known to have lower rheological properties [36, 25].

One then expects two sources of elasticity. The anchored hydrophobic parts of the proteins in the oil phase yield an elastic response, which is resisted by the viscosity of the oil. This is expected to result in an instantaneous deformation, which could be attributed to the stretching of β -sheets. The subsequent creep could be because of the uncoiling of α -helices and random coil structure and the viscous resistance arising out of internal friction of the protein domains, giving the viscoelastic effect. The secondary structure can rearrange with the conversion of α -helix into β -sheets during the deformation, and hence the plastic deformation (unrecoverable creep) can be attributed to the irreversible changes in the secondary structure of a protein membrane.

3.5 Estimation of rheological characteristics of microcapsule membrane

We first investigated surface elasticity using the approximate analysis method from the small deformation theory. In any typical electrohydrodynamic experiment, a single capsule was suspended in pure silicone oil (350 cSt) in a plastic

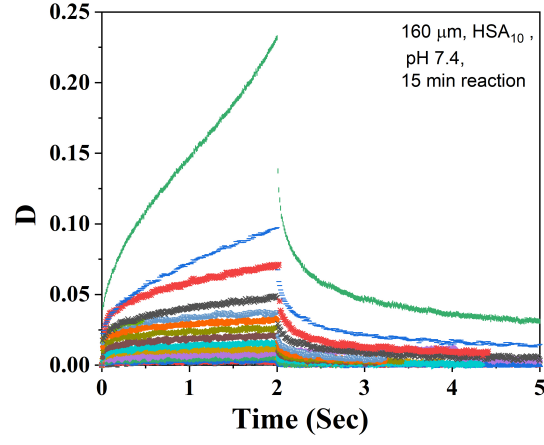


Figure 8: Dynamic deformation response HSA capsule for different electric stresses

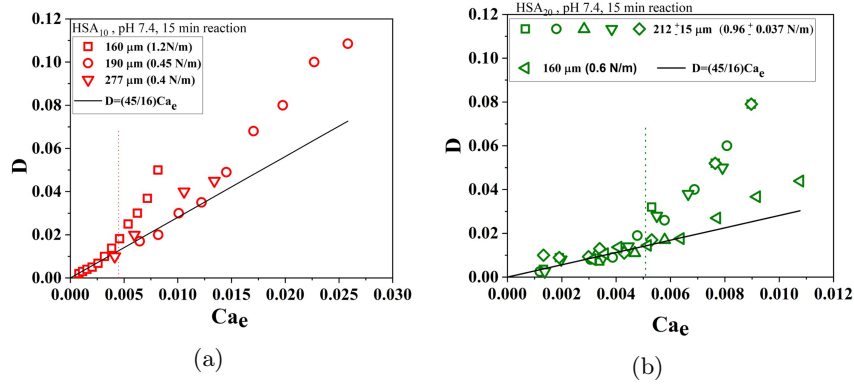


Figure 9: Deformation with respect to electric capillary number for HSA microcapsules synthesized with different HSA concentrations at pH 7.4 (a) HSA_{10} , (b) HSA_{20}

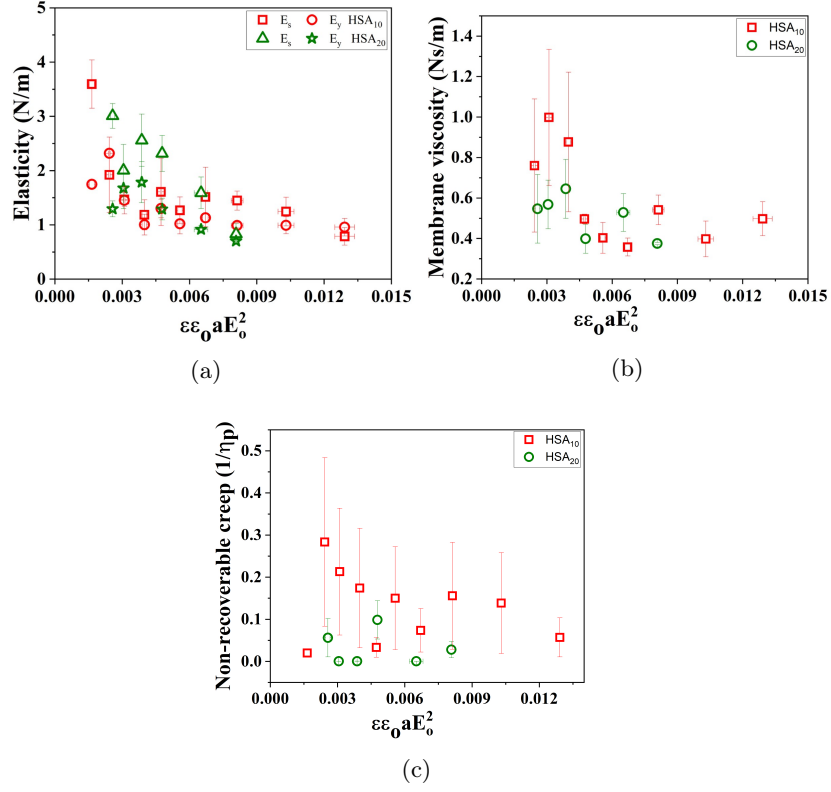


Figure 10: Interfacial rheological properties (a) elasticity, (b) membrane viscosity, and (c) unrecoverable creep at different stresses obtained from model fitting

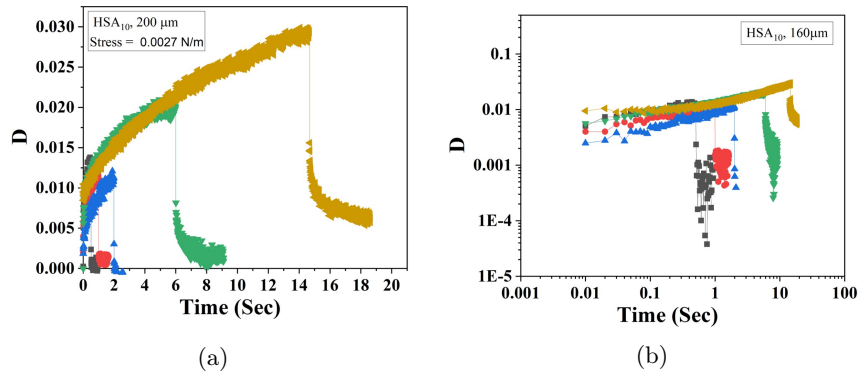


Figure 11: Dynamic deformation for HSA microcapsules suspended in 350 cSt silicone oil at constant electric field (1kHz) synthesized at pH 7.4 with 10 percent HSA concentration

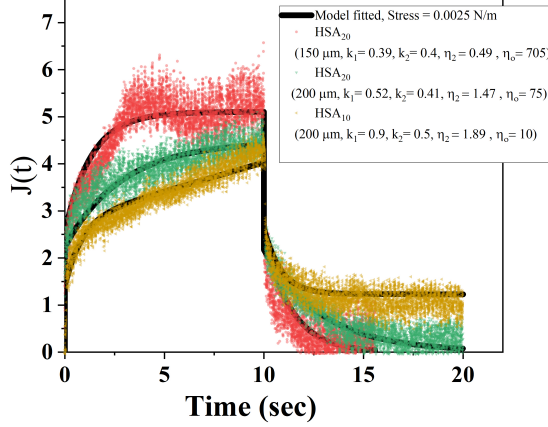


Figure 12: Creep compliance fitted with respect to time for HSA microcapsules at constant applied electric field at 1 kHz (solid line shows model fitted)

cuvette, with copper electrodes attached at its inner sidewalls, and a uniform electric field (1 kHz) was applied for about 2 s. As the electric field was switched on, the capsule was deformed to an ellipsoidal shape in the direction of an applied electric field while, after switching off the electric field, it relaxed back as shown in Figure 8. The dynamics of the deformation was studied at different electric fields until the capsule burst. The temporal data of deformation clearly shows signature of creep (Figure 8). The surface Young's modulus was calculated using the small deformation theory from the linear regime of deformation versus electric capillary number plot as shown in the Figure 9. Since the temporal deformation data shows significant creep, as a preliminary approach, we considered steady deformation value at the end of signal that is at 2 sec for computing surface elasticity by using the Eq. 2 (See [26] for details), which relates the electric capillary number (Ca_e) to deformation (D).

Figure 9 clearly shows that the HSA capsules exhibit strain-softening, for both HSA_{10} and HSA_{20} , as indicated by deviation of the D vs Ca_e curve from linearity at higher capillary numbers. This is in agreement with the observation from other studies about HSA capsules in the literature [20, 21]. A more accurate way of analysis is to fit the viscoelastic spring dashpot model to the dynamic deformation curve. Therefore, for each of the experiments in the D vs Ca_e data, a 4 element Burger model was fitted to the temporal data of deformation, and the variation of E_s , E_y , η_m and $1/\eta_p$ (unrecoverable creep) are plotted (Figure 10). The results indeed show strain softening (E_s , E_y decrease with the electric stress).

For a more detailed analysis of the viscoelastic properties of the HSA capsules, we performed creep tests using the electrodeformation method, and the Burger model described previously was fitted to compute their rheological properties.

The creep tests were performed at very low electric stress (left side of dotted lines shown in the Figure 9) to ensure that the experiments were in the linear viscoelastic regime. To get the estimate of the duration of application of electric stress required to study creep in capsules till it reaches the secondary stage, we applied constant low electric stress for the different duration as shown in Figure 11. The results indicate that applying stress for 10 sec was sufficient to study creep behaviour. Increasing the time of application of electric field could lead to large deformations, and rendering the system non-linear.

For the creep test, a low electric stress (0.0024-0.0045 N/m) was applied to the capsule suspended in 350 cSt silicone oil for 10 s. We continued video recording of electrodeformation experiments for further 10 s to capture creep recovery after switching off the field. For each experiment, a new capsule was used. The creep compliance $J(t)$, which is the ratio of deformation to stress, is plotted with respect to time for three sample data sets. The five-element spring dashpot model was fitted individually for each capsule using the MATLAB2019a as shown in Figure 12 and an excellent fit with the theoretical model was observed. The correlation between the fitted model parameters with the viscoelasto-electrohydrodynamic model was used to compute the interfacial rheological properties of HSA capsules. Following this methodology, around 76 capsules were studied using the creep test, and each data point reported was averaged over around 3-8 capsules.

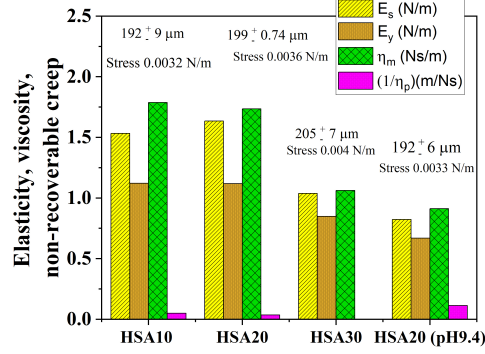
Figure 13 shows the rheological properties of HSA capsules obtained by fitting the viscoelasto-electrohydrodynamic model. Capsules $HSA_{20}, pH9.2$ synthesized with pH 9.2 buffer show low elasticity and low membrane viscosity than for the capsules HSA_{20} synthesized with phosphate 7.4 buffer with the same HSA concentration. The FTIR spectra suggests that there is greater reduction in α -helicity and a corresponding increase in the β -sheets in the case of $HSA_{20}, pH 9.2$. This is possibly due to $HSA_{20}, pH9.2$ being in the basic state, wherein it is highly charged, leading to disruption of the quarternary and tertiary structure. The highly charged HSA at pH 9.2, having greater β -sheets, could lead to increased hydrophobicity, that can cause oligomerisation in the bulk. This could result in the oligomers being weakly crosslinked at the interface, yielding lower values of the rheological parameters. This is supported by the observation of highly porous membrane in the SEM images.

We next study the effect of concentration on the rheological properties at pH 7.2. Figure 13 a shows that the surface elasticity (E_s), the membrane elasticity (E_y), the membrane viscosity (η_m), and the residual deformation (unrecoverable creep) ($1/\eta_o$) for HSA_{10} and HSA_{30} . It is found that although the concentration of HSA proteins is higher for HSA_{30} , all the rheological properties are lower than those of HSA_{10} . This is counter-intuitive, since at higher concentrations, one would have expected higher amount of crosslinking. This is infact hinted by highly folded membranes in HSA_{30} as seen from the SEM images. However, the SEM images of HSA_{30} also show significant porosity. The microscopic picture that emerges therefore suggests that the HSA_{30} in bulk water undergoes oligomerisation, leading to larger aggregates at the interface, with high porosity, resulting in capsules with much lower rheological properties.

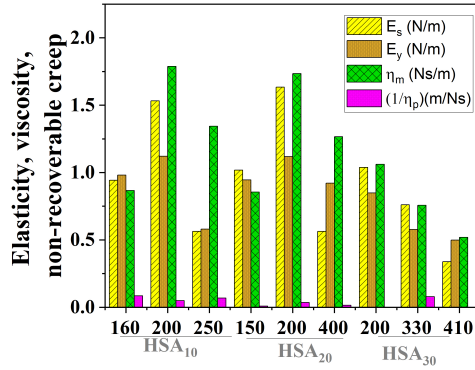
The rheological properties of HSA_{20} are similar to values of that of HSA_{10} .

HSA concentration Radius of capsule (μm)	k_1	k_2	η_2	η_o
$HSA_{10, 160}$	0.335 [0.29-0.43]	0.348 [0.297-0.43]	0.615 [0.272-1.25]	8.35 [3.5—]
$HSA_{10, 200}$	0.544 [0.44-0.675]	0.398 [0.355-0.455]	1.27 [0.7-2.05]	14.57 [10.5-25]
$HSA_{10, 250}$	0.2 [0.15-0.34]	0.2 [0.175-0.25]	0.955 [0.55-1.85]	10.32 [5.5—]
$HSA_{20} 150$	0.36 [0.26-0.53]	0.336 [0.265-0.46]	0.67 [0.13-1.75]	88.47 [8.5—]
$HSA_{20} 200$	0.544 [0.44-0.68]	0.3983 [0.355-0.455]	1.271 [0.7-2.05]	14.572 [10.5-26]
$HSA_{20} 400$	0.2 [0.145-0.33]	0.327 [0.27-0.55]	0.9 [0.57-1.84]	47.92 [8—]
$HSA_{30} 200$	0.369 [0.285-0.52]	0.3 [0.245-0.385]	0.75 [0.25-1.74]	40 [15—]
$HSA_{30} 330$	0.27 [0.225-0.375]	0.2 [0.182-0.225]	0.537 [0.3-0.99]	9 [5.5-23]
$HSA_{30} 410$	0.12 [0.095-0.21]	0.177 [0.144-0.29]	0.36888 [0.175-0.895]	22892 [8—]
$HSA_{20} \text{ pH } 9.2, 200$	0.292 [0.245-0.35]	0.237 [0.214-4.25]	0.6482 [0.38-0.98]	6.32 [4.7-8.7]

Table 1: The values of estimated model parameters for creep test with the confidence bounds in the parenthesis



(a)



(b)

Figure 13: Interfacial rheological properties elasticity (E_s , E_y) membrane viscosity (η_m), and unrecoverable creep ($1/\eta_p$) obtained from model fitting for (a) capsules synthesized with different HSA concentrations (b) for different capsule sizes and HSA concentrations.

However, the morphology of HSA_{20} is clearly more rough and folded, and even exhibits few pores. This suggests that the rheological properties of HSA_{10} and HSA_{20} could be similar because of two conflicting effects in HSA_{20} . While the crosslinking could increase because of higher bulk and thereby surface concentration of HSA_{20} , the partial bulk oligomerisation of HSA_{20} , a process akin to that discussed for HSA_{30} , could result in weak self assembly and weak crosslinking of these oligomers at the interface, resulting in a weakly elastic porous membrane. These two conflicting effects could result in HSA_{20} having similar rheological properties as HSA_{10} .

Figure 13b shows rheological properties of HSA_{10} , HSA_{20} and HSA_{30}

capsules for different sizes. Table 1 shows the values estimated model parameters and the confidence bounds for all the fitted parameters for creep test.

For both HSA_{10} and HSA_{20} , it is observed that the rheological properties, increase from a size of around 150 μm to 200 μm , whereafter, they show a decrease. This could be attributed to an increase in interfacial concentration with increase in size of the capsule. As the size of the capsule increases, the interfacial HSA concentration (molecules per unit surface area) also increases. An increase in surface concentration results in higher interfacial concentration and corresponding crosslinking of the interface, resulting in higher values of rheological properties. Table 2 shows the total interfacial concentration for 10, 20, and 30 % HSA, for capsule sizes of 150, 200, 250, 300, 350, and 400 μm . At still higher interfacial concentrations of HSA, oligomeric particles as well as a multilayered film can be formed. Moreover, the unfolding of proteins can be hindered at higher interfacial concentrations due to saturation of the interface. This can lead to reduced rheological properties.

Radius of capsule (μm)	HSA_{10} (100 mg/ml)	HSA_{20} (200 mg/ml)	HSA_{30} (300 mg/ml)
	Γ_s (molecules per nm^2)		
150	45.62	91.25	136.88
200	60.83	121.67	182.51
250	76	152	228
300	91.25	182.51	273.77
350	106.46	212.93	319.4
400	121.67	243.35	365

Table 2: The values of interfacial HSA concentration available (Γ_s) (molecules/ nm^2) for droplets of different sizes and bulk HSA concentrations

3.6 Comparison of rheological properties of HSA capsules from the literature studies

Table 3 shows a comparison of the viscoelastic properties of albumin capsules computed by different techniques as described in the literature. Table 3 shows that the elasticity increases with HSA concentration and the size of HSA capsules, which is opposite to the trend observed in our study. The difference in the results from other studies might be because studies described in the literature were done on the smaller size range, water-in-water HSA capsules with glycerol as an outer phase. After synthesizing capsules with the conventional method, they were washed and suspended in glycerol for 24 h which might have caused the morphological changes in the membrane as it is known that even after crosslinking, the HSA capsules can change their morphology when exposed to a different environment. Levy et al. [29] showed the effect of soaking highly crosslinked microcapsules obtained at pH 9.8 in a slightly alkaline buffer and hydroxylamine to destroy ester bonds, which increased the size of capsules and reduced roughness. Also, the capsules studied for the water-in-water system

could be softer with low membrane viscosity.

With a higher protein concentration, although the surface concentration is high, the interfacial adsorption and unfolding phenomena are affected by the presence of the neighboring protein molecules. At a very high protein concentration, the adsorption of protein at the interface will be faster, while in comparison the unfolding might be slower. Unfolding of protein at the interface can occur if the kinetics of adsorption is similar or slower than the kinetics of unfolding [39, 41]. Thus this could explain why while at lower concentrations, the elasticity could be lower and capsules smoother due to low bulk concentration of proteins, at very higher bulk concentration of proteins, the surface concentration could be so high that they do not unfold, and thereby the elasticity is again low. This may result in a maxima at some intermediate bulk concentration of proteins. Similarly the elasticity is expected to be higher at higher pH due to participation of carboxylic and hydroxyl groups in reaction with TC.

capsule diameter (μm)	HSA concentration (%)	Elasticity (N/m)	membrane viscosity (Ns/m)	Technique	Model used	Reference
140-310	5 – 10 – 15%	0.002-5	-	Elongational flow	small deformation theory	[12]
30-80	15-25	0.007-0.016	-	Elongational flow	Generalized Hookes law (Poisson ratio 0.4)	[13]
40-450	15-35	0.02-1	-	Elongational flow	Neo-Hookean	[21]
110-124	20-30	0.02-0.12	0.0008	shear flow	Neo-Hookean	[19]
54	20-25	-	0.00013-0.00025	tank treading shear flow	-	[14]
110-124	20	0.002-0.02	0.0008	shear	Neo-Hookean	[20]

Table 3: comparison of the viscoelastic properties of albumin capsules computed by different techniques

(Note: All studies are reported in this table with glycerol as outer fluid, with 30 min reaction time at pH 8 except the study by Gires et al. [20], which is with dragozat as outer media and 60 sec reaction time at pH 9.8)

3.7 Frequency sweep test results:

The oscillatory test was conducted on the HSA_{20} capsule suspended in 350 cSt silicone oil using the electrodeformation method described earlier. The smaller water drop was also suspended in the same cuvette for reference to get the exact estimate of time $t=0$, at which the field was switched on. Figure 14 shows dynamic deformation of drop and capsules placed in the same cuvette at 1 kHz. The deformation of water drop is scaled to match with capsule deformation in Figure 14. As the sinusoidal electric field was applied, the capsules showed oscillatory deformation. A constant low electric stress (0.0025 N/m) was applied

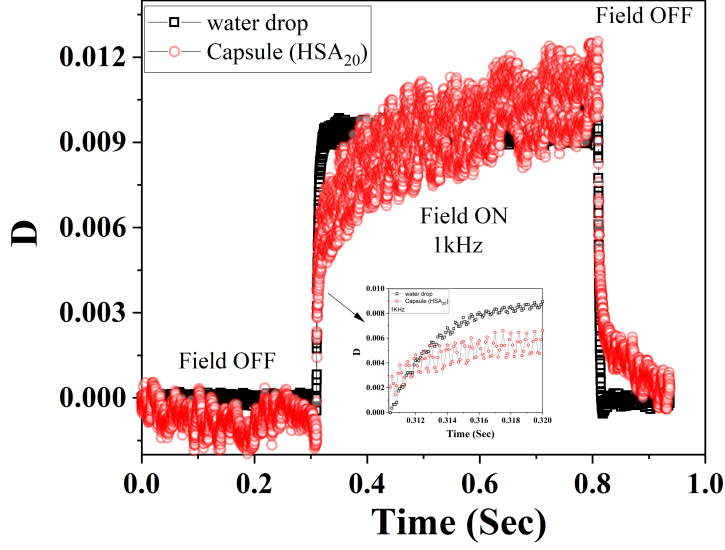


Figure 14: Dynamic deformation of drop and capsules place in the same cuvette containing 350 cSt silicone oil under constant electric field at 1kHz frequency.

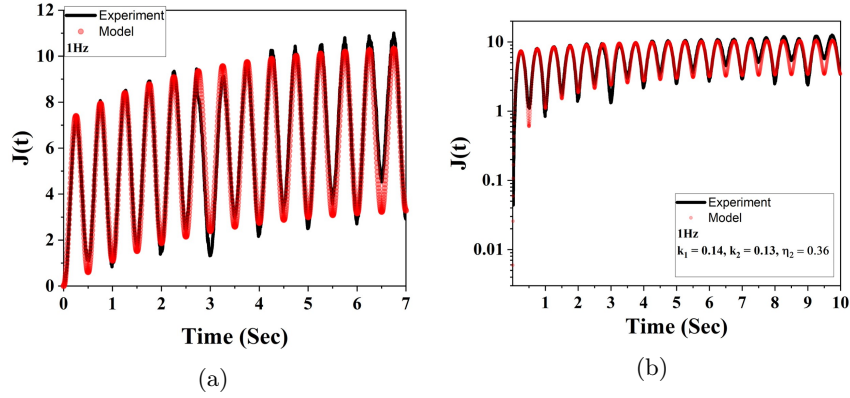


Figure 15: Oscillatory viscoelastic model fitted for (a) HSA_{20} capsule at 10 Hz (b) shows a same plot with semilog scale

at different frequencies varying from 10 Hz to 1 kHz, and the deformation video was recorded to study the effect of frequency on membrane viscoelastic properties. The dynamic deformation was fitted (Figure 15) with the model described earlier, and the membrane surface elasticity and viscosity were computed from the model parameters.

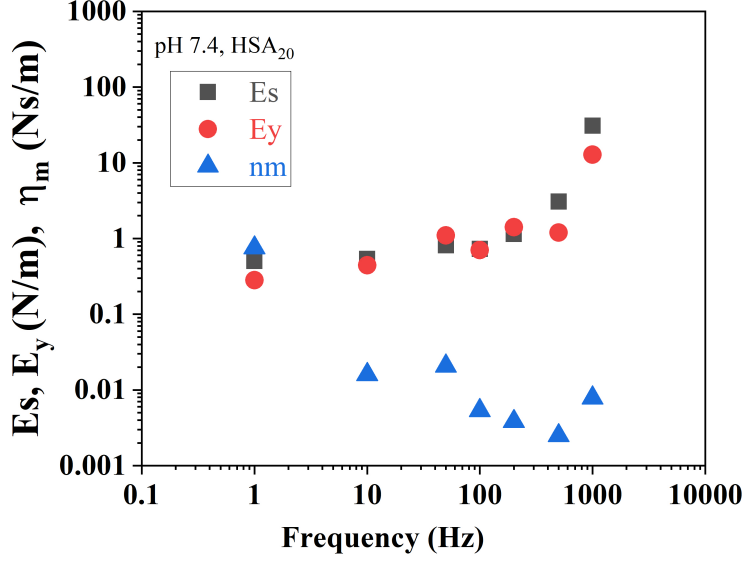


Figure 16: Variation of elasticity and membrane viscosity of HSA_{20} capsules with frequency

Figure 16 shows that as the frequency increases, the elastic modulus increases, indicating the dominance of elastic response. There are two inherent time scales in the interfacial rheology of HSA capsules, τ_1 and τ_2 , which are of the order of 1s and 1ms, thereby suggesting a crossover in properties around 1 Hz and 1 kHz.

With an increase in frequency, the timescale for viscous relaxation processes decrease, and thus the elastic response (storage modulus) shows dominance over the loss modulus. At 1 Hz, which is the lowest frequency used in the present study, both elasticity and viscosity are approximate of the same order indicating crossover frequency. This suggests that there could be irreversible structural changes in the interfacial film at lower frequencies resulting in structural breakup, which suggests at using still smaller applied stress.

4 Summary and conclusion:

The configuration of even uncrosslinked protein in the bulk solution is complex and dependent on parameters such as pH and salinity. The behavior of protein at the oil-water interface is even more complex due to the arrangement of the hydrophobic and hydrophilic parts at the oil-water interface. Therefore, it is apparent that the microstructure of crosslinked HSA at the oil-water interface could have a hierarchy of structures. The FTIR studies, although conducted on an ensemble of microcapsules of varying sizes, indicates a significant increase in the

Frequency (Hz)	K_1	K_1	η_2	η_o
1	0.18 [0.144- 0.239]	0.1 [-1.3]	0.5363 [0.265-2.3]	29612 [0.9—]
10	0.19 [0.147- 0.275]	0.158 [0.111- 0.252]	0.011 [0.00289- 0.0389]	12637 [0.146—]
50	0.288 [0.22-0.418]	0.389 [0.105-1.9]	0.0147 [0.0014- 0.11]	5585.044 [0.038—]
100	0.258 [0.228-3]	0.249 [0.186- 0.345]	0.0038 [0.0019- 0.0066]	61104 [-0.038- -]
200	0.4086 [0.362- 0.467]	0.5 [0.383- 0.685]	0.0027 [0.0011- 0.0054]	82643 [0.035- -]
500	1.093 [0.675-2.66]	0.4249 [0.245-0.78]	0.00172 [0.00045- 0.0043]	41513 [0.012- -]
1000	10.93 [7.48-20.5]	4.54 [3,37-3.55]	0.0055 [0.0011- 0.0148]	157015 [0.06 - -]

Table 4: The values of estimated model parameters for oscillatory test with the confidence bounds in the parenthesis

β sheet content at higher pH. The SEM studies indicate smoother smaller capsules, while capsules at higher pH and higher concentrations are rough. Additionally they may also have pores. EHD based interfacial rheological studies indicate that the creep and oscillatory response of the capsules can be reasonably described by the four-element Burger model, and the capsules can admit viscoelasticity as well as unrecoverable creep. Creep experiments performed on HSA capsules show that at a higher concentration of HSA, membrane with less elasticity is formed, which also shows more unrecoverable creep. Similarly, at higher pH, membranes with poor rheological properties are formed. Likewise, as the size is increased, the interfacial rheology first improves, becoming more viscoelastic, while at larger sizes, the viscoelastic properties reduce. The mechanism at play seems to be higher β sheets and thereby higher unfolding and hydrophobic oligomerisation at higher pH, whereby the loose network of oligomers at the interface leads to weaker membranes with lower rheological values at higher pH. The weak oligomeric agglomeration at the interface also leads to a porous membrane. The reduction in viscoelastic properties at higher bulk concentrations for the same size of the capsules, seems to be due to more oligomerisation at higher concentration leading to weakly crosslinked porous membranes at higher bulk concentrations, as well as due to multilayer formation resulting in weaker membranes. The

weaker rheological properties, at very larger surface concentrations (larger sizes too) is possibly due to multilayer formation and thereby weakly crosslinked membranes. On the other hand, in the low interfacial concentration regime, as the interfacial concentration increases, the rheological properties improve due to increase interfacial concentration and crosslinking. Thus, the properties seem to be dependent upon the extent of oligomerisation in the bulk; which could depend upon the pH (through hydrophobic interactions and destruction of native structure), interfacial concentration, multilayer formation, and unfolding characteristics at the interface, which depend upon the surface concentration, hydrophobic interactions, crosslinking at the interface, and the dynamics of unfolding versus adsorption. An oscillatory test was performed in the high-frequency range that shows a dominance of the elastic network at higher frequency, thereby indicating that the system might be yielding at lower frequencies.

To conclude, this work tries to establish a microstructure-rheology relationship for HSA microcapsules. Understandably, the origin of viscoelasticity in this system, although expected to be non-trivial seems to be represented by the Burger model in the kHz frequency range. The EHD method developed here for explaining high-frequency interfacial rheology therefore shows promise. A more detailed investigation would thus unravel several mysteries in this interesting system, and the work presented here could be considered to be a humble beginning in this regard.

References

- [1] Basir Ahmad, Md Zulfazal Ahmed, Soghra Khatun Haq, and Rizwan Hasan Khan. Guanidine hydrochloride denaturation of human serum albumin originates by local unfolding of some stable loops in domain iii. *Biochimica et Biophysica Acta (BBA)-Proteins and Proteomics*, 1750(1):93–102, 2005.
- [2] Dominique Barthes-Biesel and H Sgaier. Role of membrane viscosity in the orientation and deformation of a spherical capsule suspended in shear flow. *Journal of Fluid Mechanics*, 160:119–135, 1985.
- [3] ALFRED E BROWN and JOHN MENKART. Physical, chemical, and mechanical properties of protein fibers. In *Ultrastructure of Protein Fibers*, pages 5–17. Elsevier, 1963.
- [4] Markus J Buehler and Sinan Keten. Elasticity, strength and resilience: A comparative study on mechanical signatures of α -helix, β -sheet and tropocollagen domains. *Nano Research*, 1(1):63–71, 2008.
- [5] Muriel Carin, Dominique Barthès-Biesel, Florence Edwards-Lévy, Caroline Postel, and Diana Cristina Andrei. Compression of biocompatible liquid-filled hsa-alginate capsules: Determination of the membrane mechanical properties. *Biotechnology and bioengineering*, 82(2):207–212, 2003.

- [6] Nicholas Jun-An Chan, Duniy Gu, Shereen Tan, Qiang Fu, Thomas Geoffrey Pattison, Andrea J O'Connor, and Greg G Qiao. Spider-silk inspired polymeric networks by harnessing the mechanical potential of β -sheets through network guided assembly. *Nature communications*, 11(1):1–14, 2020.
- [7] S Chien, Kl L Sung, R Skalak, S Usami, and A Tözeren. Theoretical and experimental studies on viscoelastic properties of erythrocyte membrane. *Biophysical Journal*, 24(2):463–487, 1978.
- [8] Seungho Choe and Sean X Sun. The elasticity of α -helices. *The Journal of chemical physics*, 122(24):244912, 2005.
- [9] TX Chu, A-V Salsac, E Leclerc, D Barthès-Biesel, H Wurtz, and F Edwards-Lévy. Comparison between measurements of elasticity and free amino group content of ovalbumin microcapsule membranes: discrimination of the cross-linking degree. *Journal of colloid and interface science*, 355(1):81–88, 2011.
- [10] TX Chu, A-V Salsac, D Barthès-Biesel, L Griscom, F Edwards-Lévy, and E Leclerc. Fabrication and in situ characterization of microcapsules in a microfluidic system. *Microfluidics and nanofluidics*, 14(1-2):309–317, 2013.
- [11] Alexey Chubarov, Anna Spitsyna, Olesya Krumkacheva, Dmitry Mitin, Daniil Suvorov, Victor Tormyshev, Matvey Fedin, Michael K Bowman, and Elena Bagryanskaya. Reversible dimerization of human serum albumin. *Molecules*, 26(1):108, 2020.
- [12] Clément de Loubens, Julien Deschamps, Marc Georgelin, Anne Charrier, Florence Edwards-Levy, and Marc Leonetti. Mechanical characterization of cross-linked serum albumin microcapsules. *Soft matter*, 10(25):4561–4568, 2014.
- [13] Clement De Loubens, Julien Deschamps, Gwenn Boedec, and Marc Leonetti. Stretching of capsules in an elongation flow, a route to constitutive law. *Journal of Fluid Mechanics*, 767, 2015.
- [14] Clement De Loubens, Julien Deschamps, Florence Edwards-Lévy, and Marc Leonetti. Tank-treading of microcapsules in shear flow. *Journal of Fluid Mechanics*, 789:750–767, 2016.
- [15] Elizabeth P DeBenedictis and Sinan Keten. Mechanical unfolding of alpha- and beta-helical protein motifs. *Soft matter*, 15(6):1243–1252, 2019.
- [16] André C Dumetz, Aaron M Chockla, Eric W Kaler, and Abraham M Lenhoff. Effects of ph on protein–protein interactions and implications for protein phase behavior. *Biochimica et Biophysica Acta (BBA)-Proteins and Proteomics*, 1784(4):600–610, 2008.

- [17] John D’Errico. fminsearchbnd, fminsearchcon–file exchange–matlab central, 2012.
- [18] F Edwards-Lévy, M-C Andry, and M-C Lévy. Determination of free amino group content of serum albumin microcapsules using trinitrobenzenesulfonic acid: effect of variations in polycondensation ph. *International journal of pharmaceutics*, 96(1-3):85–90, 1993.
- [19] Pierre-Yves Gires, Dominique Barthès-Biesel, Eric Leclerc, and Anne-Virginie Salsac. Transient behavior and relaxation of microcapsules with a cross-linked human serum albumin membrane. *Journal of the mechanical behavior of biomedical materials*, 58:2–10, 2016.
- [20] PY Gires, AV Salsac, E Leclerc, F Edwards-Lévy, D Barthès-Biesel, et al. Mechanical characterisation of reticulated albumin capsule membranes. *4th Micro and Nano Flows Conference (MNF2014)*, 2014.
- [21] Jonathan Gubspun, Pierre-Yves Gires, Clément de Loubens, Dominique Barthès-Biesel, Julien Deschamps, Marc Georgelin, Marc Leonetti, Eric Leclerc, Florence Edwards-Lévy, and Anne-Virginie Salsac. Characterization of the mechanical properties of cross-linked serum albumin microcapsules: effect of size and protein concentration. *Colloid and Polymer Science*, pages 1–9, 2016.
- [22] Rui Han, Xianfeng Wang, Guangming Zhu, Ningxu Han, and Feng Xing. Investigation on viscoelastic properties of urea-formaldehyde microcapsules by using nanoindentation. *Polymer Testing*, 80:106146, 2019.
- [23] Jen Hsin, Johan Strümpfer, Eric H Lee, and Klaus Schulten. Molecular origin of the hierarchical elasticity of titin: simulation, experiment, and theory. *Annual review of biophysics*, 40:187–203, 2011.
- [24] Kiyoshi Inokuchi. Rheology of surface films. i. rheological characteristics of monomolecular films of ovalbumin and serum albumin. *Bulletin of the Chemical Society of Japan*, 26(9):500–506, 1953.
- [25] J Jancar. The thickness dependence of elastic modulus of organosilane interphases. *Polymer Composites*, 29(12):1372–1377, 2008.
- [26] Rahul B Karyappa, Shivraj D Deshmukh, and Rochish M Thaokar. Deformation of an elastic capsule in a uniform electric field. *Physics of Fluids*, 26(12):122108, 2014.
- [27] Keekyoung Kim, Xinyu Liu, Yong Zhang, Ji Cheng, Xiao Yu Wu, and Yu Sun. Elastic and viscoelastic characterization of microcapsules for drug delivery using a force-feedback mems microgripper. *Biomedical Microdevices*, 11(2):421, 2009.

- [28] Yannick Lefebvre, Eric Leclerc, Dominique Barthès-Biesel, Johann Walter, and Florence Edwards-Lévy. Flow of artificial microcapsules in microfluidic channels: A method for determining the elastic properties of the membrane. *Physics of Fluids (1994-present)*, 20(12):123102, 2008.
- [29] Marie-Christine Levy, Sandrine Lefebvre, Miloud Rahmouni, Marie-Christine Andry, and Michel Manfait. Fourier transform infrared spectroscopic studies of human serum albumin microcapsules prepared by interfacial cross-linking with terephthaloylchloride: Influence of polycondensation ph on spectra and relation with microcapsule morphology and size. *Journal of pharmaceutical sciences*, 80(6):578–585, 1991.
- [30] Marie-Christine Levy, Marie-Christine Andry, Sandrine Lefebvre, and Michel Manfait. Fourier transform infrared spectroscopic studies of cross-linked human serum albumin microcapsules. 3. influence of terephthaloyl chloride concentration on spectra and correlation with microcapsule morphology and size. *Journal of pharmaceutical sciences*, 84(2):161–165, 1995.
- [31] Jen-Jen Lin, Jeffrey D Meyer, John F Carpenter, and Mark C Manning. Stability of human serum albumin during bioprocessing: denaturation and aggregation during processing of albumin paste. *Pharmaceutical research*, 17(4):391–396, 2000.
- [32] Tao Lin, Zhen Wang, Ruixin Lu, Wen Wang, and Yi Sui. A high-throughput method to characterize membrane viscosity of flowing microcapsules. *Physics of Fluids*, 33(1):011906, 2021.
- [33] Rustem I Litvinov, Dzhigangir A Faizullin, Yuriy F Zuev, and John W Weisel. The α -helix to β -sheet transition in stretched and compressed hydrated fibrin clots. *Biophysical journal*, 103(5):1020–1027, 2012.
- [34] Ashutosh Namdeo, Jainesh H Jhaveri, SM Mahajani, and AK Suresh. Palladium catalyzed liquid phase oxidation of glycerol under alkaline conditions-kinetic analysis and modelling. *Chemical Engineering Journal*, 438:135424, 2022.
- [35] Sneha Puri and Rochish Thaokar. Study of the effect of hydrolysis time on the mechanical properties of polysiloxane microcapsules. *Langmuir*, 38(12):3729–3738, 2022.
- [36] Sneha Puri and Rochish M Thaokar. Study of dependence of elasticity on the microstructure of microcapsules using electro-deformation technique. *Colloids and Surfaces A: Physicochemical and Engineering Aspects*, 569:179–189, 2019.
- [37] Bal Ram Singh, Daniel B DeOliveira, Fen-Ni Fu, and Michael P Fuller. Fourier transform infrared analysis of amide iii bands of proteins for the secondary structure estimation. In *Biomolecular spectroscopy III*, volume 1890, pages 47–55. International Society for Optics and Photonics, 1993.

- [38] Dmitrii Usoltsev, Vera Sitnikova, Andrey Kajava, and Mayya Uspenskaya. Ftir spectroscopy study of the secondary structure changes in human serum albumin and trypsin under neutral salts. *Biomolecules*, 10(4):606, 2020.
- [39] Peter A Wierenga, Maarten R Egmond, Alphons GJ Voragen, and Harmen HJ de Jongh. The adsorption and unfolding kinetics determines the folding state of proteins at the air–water interface and thereby the equation of state. *Journal of colloid and interface science*, 299(2):850–857, 2006.
- [40] Huayan Yang, Shouning Yang, Jilie Kong, Aichun Dong, and Shaoning Yu. Obtaining information about protein secondary structures in aqueous solution using fourier transform ir spectroscopy. *Nature protocols*, 10(3):382–396, 2015.
- [41] Yohko F Yano. Kinetics of protein unfolding at interfaces. *Journal of Physics: Condensed Matter*, 24(50):503101, 2012.
- [42] Alireza Yazdani and Prosenjit Bagchi. Influence of membrane viscosity on capsule dynamics in shear flow. *Journal of Fluid Mechanics*, 718:569–595, 2013.
- [43] Chunyu Zhang, Yanli Xie, and Junjun Zou. Effect of the viscoelastic properties of modified starch as a wall material on the surface morphology of microcapsules. *Journal of the Science of Food and Agriculture*, 99(10):4725–4730, 2019.
- [44] Yulin Zhang, Chengxin Hu, Xu Xiang, Yongfu Diao, Binwei Li, Linying Shi, and Rong Ran. Self-healable, tough and highly stretchable hydrophobic association/ionic dual physically cross-linked hydrogels. *RSC advances*, 7(20):12063–12073, 2017.

Supplementary Information: Study of Interfacial Rheology of Human Serum Albumin Microcapsules using Electrodeformation Technique

Capsules size distribution

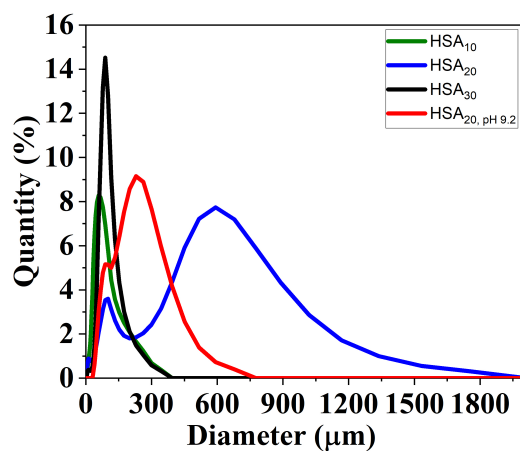


Figure S1: Size distribution for HSA capsules synthesized at 600 rpm with different HSA concentrations and pH

Figure S1 shows the size distribution of HSA capsules studied by using a particle size analyzer (Horiba). The outer organic phase (cyclohexane) was replaced by deionized water by decanting the oil phase and successively washing capsules with deionized water. Finally, capsules were suspended in the deionized water for studying particle size distribution.

While the size distribution for HSA_{10} and HSA_{30} is unimodal, the one for HSA_{20} for both phosphate and carbonate buffers is bimodal. The smaller capsules were formed in the range of 100-150 μm for all the four cases. For HSA_{20} , and $HSA_{20,9.2}$, which show bimodal distribution, the 2nd peak is seen around a size range of 300 and 600 μm respectively. It is unclear if the 2nd peak for HSA_{20} is due to agglomeration of capsules or if the distribution is really bimodal. The electrohydrodynamic experiments to determine the rheology of the capsules were conducted on one single capsule at-a-time, chosen from these distributions. It should be remembered that these distributions themselves are for water-in-water HSA capsules, while the EHD experiments were conducted on water-in-oil HSA capsules.

A number of factors determine the size distribution of these capsules. The size distribution of a water-in-oil emulsion depends upon the interfacial tension and surface elasticity of the resulting droplets. While the system starts as an

emulsion of water droplets in oil, coated with HSA and stabilized by surfactant (span 85), it soon undergoes interfacial condensation, which can possibly both prevent breakup as well as prevent coalescence of the resulting capsules. This complex interplay of uncrosslinked droplets and crosslinked capsules, could be responsible for the resulting size distribution of the capsules. While higher concentration of HSA can reduce the interfacial tension, it can also increase the interfacial elasticity of the interface.

Characterization of capsules using Fourier transform infrared spectroscopy (FTIR) technique:

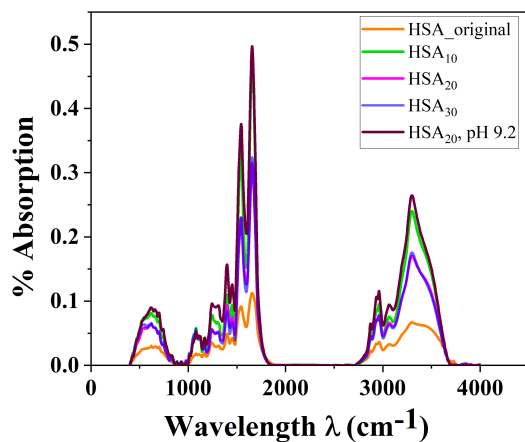


Figure S2: Full range FTIR spectra for original lyophilized HSA (without crosslinked) and for HSA capsules synthesized at different reaction conditions

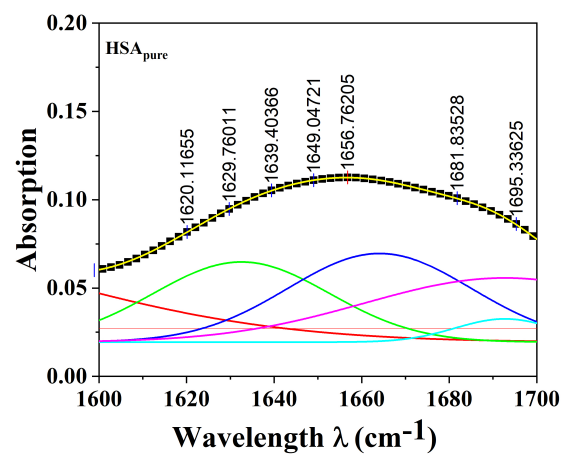


Figure S3: The Amide I band and its second derivative deconvolution fitted for original uncrosslinked HSA

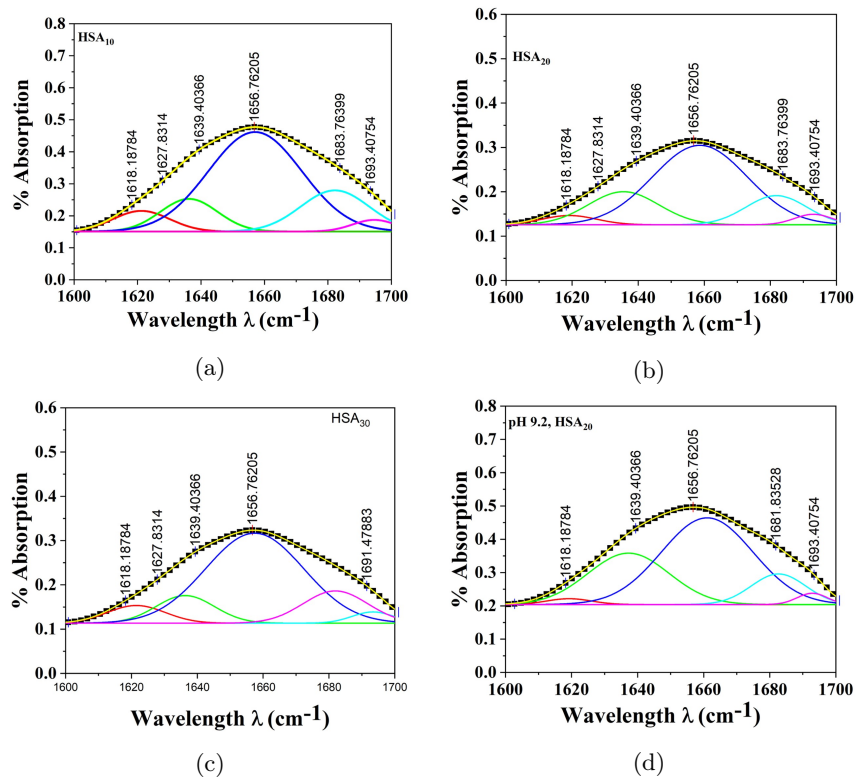


Figure S4: The Amide I band and its second derivative deconvolution fitted for capsules prepared with 15 min reaction time with phosphate pH 7.4 buffer (a) HSA_{10} (b) HSA_{20} (c) HSA_{30} , (d) $\text{HSA}_{20}, \text{pH } 9.2$